2 (2026) 100117

Contents lists available at ScienceDirect

NAM Journal

journal homepage: www.sciencedirect.com/journal/nam-journal

R3ACT: An Oxygen-Controlled Biosensor-Based NAM to Support Animal-Free Chemical Safety Assessment

Joudi Armouch [a,b], Hamzah Issa [a,c], Emre Vatandaşlar [a,d], Sena Yildirim [a,c], Seyed Mohammad Miri [a,c], Asel Aydeger [a,c], Asal Ghaffari Zaki [a,c], Melike Secilmis [e], Kıvanç Kök [a,f,g], Ahmet Kaplan [a,g], Theresa Balber [h,i], Thomas Birngruber [j], Ahmet Katı [k,l], Emrah Eroglu [a,m,*]

[a] Research Institute for Health Sciences and Technologies (SABITA), Istanbul Medipol University, Istanbul, 34810, Türkiye
[b] Biomedical Engineering and Bioinformatics, Graduate School of Engineering and Natural Sciences, Istanbul Medipol University, Istanbul, 34810, Türkiye
[c] Graduate School of Health Sciences, Istanbul Medipol University, Istanbul, 34810, Türkiye
[d] Department of Histology and Embryology, Faculty of Medicine, Istanbul Medipol University, 34810, Türkiye
[e] Department of Basic Medical Sciences, Atlas University, Istanbul, 34403, Türkiye
[f] Department of Biostatistics and Medical Informatics, International School of Medicine, Istanbul Medipol University, Istanbul, 34810, Türkiye
[g] Multi-Omics Design and Analysis Studio (MODAS-SABITA), Istanbul Medipol University, Istanbul, 34810, Türkiye
[h] Joint Applied Medicinal Radiochemistry Facility, University of Vienna, Medical University of Vienna, Vienna, Austria
[i] Division of Nuclear Medicine, Department of Biomedical Imaging and Image-Guided Therapy, Medical University of Vienna, Vienna, Austria
[j] HEALTH – Institute for Biomedical Research and Technologies, Joanneum Research Forschungsgesellschaft mbH, Graz, 8010, Austria
[k] Center for Targeted Therapy Technologies, Bogazici University, Istanbul, Türkiye
[l] Experimental Medicine Research and Application Center, University of Health Sciences, Istanbul, Türkiye
[m] Molecular Biology, Genetics, and Bioengineering Program, Sabanci University, Istanbul 34956, Türkiye

ARTICLE INFO

Keywords:
New Approach Methodologies
Animal-free chemical safety assessment
Physiological oxygen
Redox biology
Nrf2

ABSTRACT

Most in vitro chemical safety workflows are performed in ambient air, although many human tissues experience substantially lower physiological oxygen levels. This mismatch can alter redox tone, stress-response signaling, and interpretation of chemical effects. Here, we present R3ACT (Redox & Antioxidant Capacity Tracker), an animal-free, oxygen-controlled live-cell NAM for mechanistic profiling of redox perturbation and antioxidant-response activation. In human HaCaT keratinocytes adapted to 5 kPa O_2, R3ACT combines viability-gated concentration selection, oxygen-controlled plate-reader measurements, high-content microscopy, and deep-learning-assisted single-cell analysis. The workflow integrates cytosolic and mitochondrial HyPer7.2 biosensors for H_2O_2 dynamics with POINTER, an Nrf2 transcriptional reporter, to assess antioxidant-response engagement. As proof of concept, four exposure-relevant materials were profiled in the main screen, with iron formulations assessed as additional pharmaceutical case examples. Zinc oxide produced the strongest reproducible Nrf2 activation across two independent runs, confirmed by single-cell microscopy. Polystyrene nanoplastics likewise showed reproducible, microscopy-confirmed Nrf2 activation, whereas perfluorooctanoic acid showed a borderline response that was not confirmed by microscopy. Salicylic acid induced Nrf2 activation under physiological oxygen and was interpreted as antioxidant-response engagement rather than skin-sensitization classification. HyPer7.2 provided compartment-specific mechanistic context, but often revealed transient fluctuations rather than consistent material-induced H_2O_2 increases. Together, these data position R3ACT as an early-stage, oxygen-controlled NAM that may support animal-free chemical and drug-screening workflows by generating mechanistic redox/Nrf2 response profiles for compound prioritization. Further benchmarking, predefined performance criteria, and inter-laboratory studies are required before regulatory applicability can be assessed.

* Corresponding author at: SABITA – Istanbul Medipol University.
E-mail address: emrah.eroglu@medipol.edu.tr (E. Eroglu).

https://doi.org/10.1016/j.namjnl.2026.100117
Received 15 May 2026; Received in revised form 6 July 2026; Accepted 19 July 2026
Available online 19 July 2026

Introduction

Safety assessment aims to identify and mitigate potential toxic effects of chemicals, pharmaceuticals, and consumer products to protect human health and the environment. Traditionally, this process has relied heavily on animal models (Kimber and Weisenberger, 1989). This approach raises ethical concerns and suffers from limited cross-species predictivity, high costs, and low throughput (Schmeisser et al., 2023). The principles of Replacement, Reduction, and Refinement (3Rs) established a foundation for more humane and scientifically sound testing strategies (Hubrecht and Carter, 2019). Regulatory actions have further accelerated this transition, including the EU ban on animal testing for cosmetics and the REACH regulation (Fischer, 2015; Fentem et al., 2021). More recently, the U.S. FDA Modernization Act 2.0 formally enabled the use of non-animal methods in drug development (Han, 2023). Together, these developments have driven the adoption of New Approach Methodologies (NAMs), such as in silico models, high-throughput screening, and advanced in vitro systems, to support next-generation risk assessment (Schmeisser et al., 2023).

Keratinocytes are relevant sentinels for chemical exposure because skin is a major interface with consumer products, cosmetics, environmental chemicals, and pharmaceutical formulations. Existing keratinocyte-based NAMs have contributed substantially to non-animal safety assessment, particularly through pathway-focused readouts such as Keap1–Nrf2 activation in KeratinoSens™ and LuSens™ assays (Emter et al., 2010; Ramirez et al., 2014, 2016; OECD, 2024, 2025). However, for roadmap-oriented animal-free chemical safety assessment, there is a complementary need for mechanistic workflows that do not only classify a single endpoint but also provide interpretable information on early cellular stress biology. In this context, redox perturbation and antioxidant-response activation are useful mechanistic dimensions because they can inform compound prioritization, follow-up testing, and NGRA-oriented (Next-Generation Risk Assessment) weight-of-evidence assessment. This transition is now moving from isolated method development toward roadmap-based implementation, where NAMs must provide reproducible, interpretable, and human-relevant evidence that can support chemical safety decisions across sectors. While many in vitro methods represent major advances, they rely on a single functional readout that captures antioxidant pathway activation without parallel information on the underlying intracellular redox state (Nwachukwu et al., 2021; Murphy et al., 2022). Consequently, redox perturbations and adaptive antioxidant responses cannot be disentangled, limiting mechanistic insight and interpretability (Murphy et al., 2022). An improved strategy would therefore integrate complementary readouts that report on both intracellular redox dynamics and downstream antioxidant capacity.

A critical, yet often underappreciated, determinant of redox biology in vitro is oxygen tension (Keeley and Mann, 2019). Oxygen level is a key regulator of cellular physiology, redox balance, and stress-response signaling (Stuart et al., 2018). Culture under supraphysiological oxygen conditions can disrupt redox homeostasis, increase reactive oxygen species (ROS) formation, alter mitochondrial function, and activate non-physiological stress pathways, thereby modifying cellular sensitivity to pharmacological compounds (Tiede et al., 2011; Stuart et al., 2018; Sevimli et al., 2022; Altun et al., 2024; Barakat et al., 2025; Miri et al., 2025). This is particularly relevant for skin-based in vitro models, as epidermal and dermal cells normally reside in low-oxygen microenvironments. Appropriate oxygen control may therefore improve physiological relevance and reduce oxygen-driven artifacts in non-animal test systems (Chettouh-Hammas and Grillon, 2024).

Despite the rapid expansion of NAMs, many screening workflows still depend on simplified endpoint measurements (e.g., viability or a single marker at a single time point), which can miss early hazard signals, constrain mechanistic interpretation, and weaken confidence in translating in vitro findings to human risk (Franzosa et al., 2021; Lu, 2024). Genetically encoded fluorescent biosensors are well aligned with NAM principles because they enable time-resolved, multiparametric readouts in human-relevant cell models, supporting more information-rich decision-making in toxicology and drug discovery (Potekhina et al., 2020). Yet, despite their utility, biosensors are not routinely integrated into standard screening pipelines to the same extent as conventional assays (Eroğlu, 2024). Redox biosensors demonstrate how compounds and xenobiotics can be evaluated for oxidative stress liabilities directly in living cells, and ongoing sensor engineering continues to expand screening-ready reporters for cellular stress and metabolism (Pang et al., 2021). Importantly, this direction is reinforced by regulatory momentum: the FDA is explicitly advancing alternative methods/NAMs to improve predictivity while reducing animal use, and recent policy-focused discussions highlight accelerating adoption of such approaches for safety assessment (Westmoreland et al., 2022).

Building on this concept, we introduce R3ACT (Redox & Antioxidant Capacity Tracker), an oxygen-controlled, biosensor-based NAM for mechanistic profiling of chemical-induced redox perturbation and Nrf2-dependent antioxidant-response activation. R3ACT combines HyPer7.2 (Pak et al., 2020), a genetically encoded reporter of intracellular H_2O_2 dynamics, with POINTER (Miri et al., 2025), an oxygen-insensitive Nrf2 transcriptional reporter for antioxidant-response engagement. R3ACT is intended as an early-stage animal-free screening and prioritization workflow for chemical safety assessment. The present study establishes the feasibility of integrating physiological oxygen control, live-cell biosensors, viability-gated concentration selection, high-throughput screening, high-content microscopy, and deep-learning-assisted single-cell analysis into a roadmap-relevant NAM workflow.

2. Materials and Methods

2.1. Cell Culture

HaCaT human keratinocytes (cat. no. 300493, Cytion, Germany) were maintained according to the manufacturer's recommendations. Cells were cultured in high-glucose Dulbecco's Modified Eagle Medium (DMEM; Gibco, USA) supplemented with 10% fetal bovine serum (FBS; Wisent, Canada) and 1 × antibiotic–antimycotic (Gibco, USA). For passaging, Trypsin/EDTA (0.25% trypsin, 0.1% EDTA) with phenol red and Dulbecco's PBS without Ca^{2+}/Mg^{2+} were used. Cells were kept at 37°C in a humidified atmosphere. Under room-air conditions, cells were maintained in an incubator set to 5% CO_2. For physiological oxygen conditions, cells were cultured in an oxygen-regulated incubator set to 5% CO_2 and 5% O_2. To support adaptation to physiological oxygen levels, cells were cultured at 5% O_2 for at least 5 days before experimentation. Cells were routinely passaged at 70–80% confluence. For live-cell imaging–based reporter characterization, cells were seeded into 6-well plates containing 30-mm No. 1 glass coverslips (Glaswarenfabrik Karl Knecht Sondheim, Germany). For high-content microscopy confirmation of selected plate reader responses, approximately 50,000 cells per well were seeded onto 24-well glass-bottom plates (cat. no. 801006, NEST, China). The current workflow used FBS-containing medium to maintain comparability with standard HaCaT culture conditions. Because FBS is animal-derived, future refinement of R3ACT will evaluate chemically defined or human-derived alternatives, including serum-free keratinocyte media, human serum, or human platelet lysate, while monitoring viability, reporter baseline, oxygen adaptation, and biosensor dynamic range.

2.2. Generation of Stable Cell Lines

Cells were used between passages 25-40 after thawing. Cell identity was based on the documented cell source (cat. no. 300493, Cytion, Germany). Additional in-house Short Tandem Repeat (STR) profiling test authentication was not performed before the present experiments. The HyPer7.2 plasmid was a kind gift from Vsevolod Belousov, whereas the POINTER sensor was recently developed in our laboratory (Miri

et al., 2025). HyPer7.2 was used in both cytosolic (NES-tagged) and mitochondria-targeted variants. For stable expression, pLenti-based vectors encoding the biosensors were used, and lentiviral particles were produced by transient co-transfection of HEK 293T packaging cells with the transfer vector and standard packaging plasmids as described previously (Secilmis et al., 2021). In brief: viral supernatants were collected and purified by sucrose cushion ultracentrifugation to concentrate viral particles. Purified lentivirus was then used to transduce target cells in the presence of polybrene (Sigma-Aldrich, USA) at a final concentration of 10 μg/mL to enhance infection efficiency. Following lentiviral transduction, biosensor-expressing cells were enriched by fluorescence-activated cell sorting (FACS) using a BD Influx Cell Sorter (BD Biosciences, USA). Cells were first gated based on forward- and side-scatter parameters to exclude debris and aggregates, and sensor-positive populations were subsequently identified and sorted using a 488 nm laser and a 530/40 nm band-pass filter, with gates defined relative to non-transduced control cells. Sorted cells were expanded and used for subsequent experiments. Post-sort enrichment was confirmed by FACS profiles (Supplementary Fig. S1) and fluorescence microscopy, but absolute post-sort purity was not quantified for the HyPer7.2 and POINTER reporter lines.

2.3. Buffers and Solutions

All chemicals were purchased from NeoFroxx (Germany), exceptions are stated respectively. Live-cell imaging was performed in HEPES-buffered saline containing 2 mM $CaCl_2$, 5 mM KCl (cat. no. 960.033.1000, ISOLAB, Germany), 138 mM NaCl (cat. no. 106404.1000, Merck, Germany), 1 mM $MgCl_2$, 10 mM HEPES, and 10 mM D-glucose (cat. no. 600-035 LG, Wisent, Canada). The pH was adjusted to 7.42 with 1 M NaOH. Stock solutions of H_2O_2 were freshly prepared in imaging buffer. Auranofin (cat. no. 15316, Cayman Chemical, USA) and perfluorooctanoic acid (PFOA; cat. no. T9333, TargetMol, USA) were dissolved in DMSO to prepare 7.37 mM and 100 mM stock solutions, respectively. Polystyrene-based nanoparticles (cat. no. 43302-5ML-F, Sigma-Aldrich, USA) were used directly after resuspension in cell culture medium. Salicylic acid (cat. no. 247588, Sigma-Aldrich, USA) was prepared as a 15 mM stock solution in culture medium. Zinc oxide (ZnO, cat. no. 108849, MERCK, Germany) was prepared as a 1 mg/mL stock solution in acidic PBS, followed by pH adjustment to 7.4. Iron sucrose (IS, Venofer®, Abdi Ibrahim Pharmaceuticals, Türkiye) and ferric carboxymaltose (FCM, Inferject®, Abdi Ibrahim Pharmaceuticals, Türkiye) were prepared as 2 mg/mL and 5 mg/mL working solutions in culture medium, respectively. A vehicle-control experiment was performed using 1% DMSO for 6 h and 24 h, corresponding to the HyPer7.2 and POINTER assay time points, respectively. Under these conditions, 1% DMSO did not alter the measured HyPer7.2 or POINTER responses compared with untreated controls. Final DMSO concentrations did not exceed 1% DMSO unless explicitly stated. For compounds prepared directly in culture medium, medium-only controls were included.

2.4. Live-Cell Imaging

Live-cell fluorescence imaging was carried out using a Zeiss Axio Observer Z1.7 inverted widefield epifluorescence microscope (Carl Zeiss AG, Germany) equipped with Plan-Apochromat 20 × /0.8 NA dry and Plan-Apochromat 40 × /1.4 NA oil-immersion objectives, and an Axiocam 503 monochrome CCD camera, and camera binning was set to 4 × 4. For characterization of HyPer7.2 dynamics, cells were stimulated with 100 μM H_2O_2 during time-lapse imaging, acquired at 3-s intervals. As light emitting diode (LED) light sources, either Cool LED or Colibri 5/7 was used and exposure time usually ranged between 50 to 800 ms according to the expression rate and fluorescence intensity. Imaging was performed in a perfusion chamber (NGFI, Graz) connected to a custom pump-driven perfusion system enabling rapid buffer exchange. For visualization of HyPer7.2, excitation was alternated between 423/44 nm and 469/38 nm using a motorized filter wheel equipped with FT455 and FT495 dichroic beamsplitters, corresponding to the HyPer "low" and "high" excitation channels. Emission was collected through a 525/50 nm bandpass filter, allowing ratiometric quantification of H_2O_2-dependent fluorescence changes. For detection of Nrf2 activity using the POINTER biosensor, excitation was set to 480 nm and emission was recorded at 525 nm. All imaging experiments were performed in a custom in-house oxygen-regulated glove box using a Zeiss A-Plan 40 × /0.65 NA air objective, except for microscopy confirmation of selected responses, for which a Zeiss C-Apochromat 40 × /1.2 NA water-immersion objective was used. System control and fluorescence data acquisition were performed using ZEN Blue 3.1 Pro software (Carl Zeiss AG).

For co-localization of HyPer7.2 and MitoTracker Red and Hoechst, a laser scanning confocal microscope (LSM 880, Carl ZEISS) equipped with a Plan-Apochromat 40x/1.3NA oil immersion objective, 380 nm, 488 nm, 594 nm excitation lasers, and Airyscan detector for Hoechst, GFP, and MitoTracker, respectively was used. To stain mitochondria and nuclei, cells were incubated with 100 nM MitoTracker Red CMXRos (Thermofisher) and 1,5 μM Hoechst 33342 (Hello Bio, HB0787), respectively in imaging buffer for 10 minutes at 37°C and washed afterward with imaging buffer.

2.5. Cell Viability Assay

Cell viability was assessed by flow cytometry using TO-PRO-3 Iodide stain (Thermo Fisher Scientific, USA) as a membrane-impermeant dead-cell marker. Cells were seeded at a density of 50,000 cells per well in 24-well plates and allowed to attach and recover for 2 days, followed by 24 h treatment with auranofin (AF; 0, 3, 5, 6, 7, 8, 10, 20 μM), perfluorooctanoic acid (PFOA; 0, 10, 30, 50, 100, 300, 500, 1000 μM), polystyrene nanoplastic (PS-NP; 0, 5, 10, 30, 50, 100, 300, 500 μL/mL), bulk ZnO (0, 3, 5, 10, 30, 50, 100, 200 μg/mL), or salicylic acid (0, 0.1, 0.3, 0.5, 1, 2, 3, 5 mM). Following treatment, culture supernatant was collected and cells were washed with 300 μl PBS, trypsinized, added to the collected supernatant, and centrifuged at 300 × g for 5 minutes. The resulting cell pellets were resuspended in FACS buffer (5% FBS in PBS), and TO-PRO-3 was added to a final concentration of 50 nM. Samples were incubated on ice for 5–10 minutes immediately prior to acquisition. Flow cytometry was performed using a BD FACSymphony A1 Cell Analyzer equipped with a 640 nm red laser, and TO-PRO-3 fluorescence was detected in the far-red channel. Cellular debris and doublet cells were excluded by FSC vs SSC and FSC-A vs FSC-H respectively. Cell viability was determined based on TO-PRO-3 exclusion, with TO-PRO-3–positive cells classified as non-viable. Data were analyzed using FlowJo (10.10.0), and percentage viability was calculated by normalizing the fraction of TO-PRO-3–negative cells in each condition to the corresponding control group.

2.6. R3ACT pilot characterization and proof-of-concept response classification

Reporter kinetics were first characterized in pilot experiments using auranofin (AF) and exogenous H_2O_2 to define suitable measurement windows for the R3ACT workflow. Based on these experiments, HyPer7.2 responses were assessed after 6 h treatment and POINTER/Nrf2 responses after 24 h treatment. AF experiments were performed under both room-air and 5 kPa O_2 conditions to evaluate oxygen-dependent reporter behavior, whereas subsequent proof-of-concept screening experiments were performed in cells adapted to 5 kPa O_2.

For proof-of-concept R3ACT screening, cells stably expressing cytosolic HyPer7.2, mitochondrial HyPer7.2, or POINTER were seeded in 96-well plates at 10,000 cells per well and cultured for 2 days before treatment. Concentration ranges (Table 1) were selected from prior viability testing to focus on conditions with limited cytotoxicity. Unless otherwise stated, treatments and measurements were conducted at 5 kPa

Table 1
Viability-gated concentration levels used for proof-of-concept R3ACT screening. *For compounds that did not reach the corresponding cytotoxicity level within the tested range, concentrations were selected from experimentally tested non-cytotoxic concentrations rather than interpreted as true interpolated IC values. For salicylic acid, the listed concentrations should therefore be interpreted as tested non-cytotoxic concentration levels rather than confirmed IC-derived cytotoxicity levels unless supported by the fitted viability model.*

Viability-gated level (%)	1.5	3	5	7	10	20	30	50
AF (μM)	0.076	0.155	0.263	0.378	0.555	1.25	2.14	5.00
PFOA (μM)	3.31	27.03	46.01	65.79	97.12	218.53	347.61	874.10
PS-NP (μL/mL)	0.79	3.64	6.20	8.87	13.09	29.45	50.46	117.80
Salicylic acid (μM)	76.14	145.60	263.16	376.30	555.50	1250.00	2142.00	5000.00
ZnO (μg/mL)	0.89	1.81	3.08	4.41	6.51	14.65	25.11	58.58

O_2 using the atmospheric control unit.

A confirmed R3ACT response was defined as a treatment condition within the predefined low-cytotoxicity window that showed a statistically significant increase versus control in the same biosensor readout and the same response direction in two independent screening runs. Responses detected in only one run, or not reproduced in the same or adjacent concentration range, were classified as borderline and were not interpreted as confirmed responses. Where microscopy confirmation was performed, plate reader responses were considered supported only if the same readout showed a significant increase at single-cell level.

Raw values were normalized to a 0–100 scale using min–max normalization (Supplementary Note 1). Heatmap-style response summaries were generated in Python using pandas, numpy, and matplotlib. Non-significant responses are shown in grayscale to visualize response magnitude without classifying them as confirmed responses. Confirmed or borderline responses are indicated using the corresponding biosensor color code: green for HyPer7.2/H_2O_2 readouts and red for POINTER/Nrf2 readouts.

2.7. Plate-reader biosensor measurements

Fluorescence was recorded using a CLARIOstar Plus microplate reader (BMG LABTECH, Germany). For HyPer7.2, fluorescence signals corresponding to the reduced (HyPer Low) and oxidized (HyPer High) excitation states were acquired at 400/15 nm (dichroic 458.8; emission 530/40; gain 1500) and 490/15 nm (dichroic 503.8; emission 530/40; gain 2000), respectively, and the HyPer7.2 ratio was calculated as HyPer High/HyPer Low. For POINTER, measurements were acquired using excitation at 450/15 nm (dichroic 473.2; emission 499/20; gain 2200). All readouts were measured under controlled oxygen and carbon dioxide levels using the atmospheric control unit (ACU).

2.8. Statistical analysis

Statistical analyses were performed using GraphPad Prism. Data are presented as mean ± SD unless otherwise stated. For comparisons between two groups, unpaired two-tailed Student's t-tests were used. For multiple-group comparisons, one-way ANOVA followed by Dunnett's or Tukey's post hoc test was applied as indicated. For oxygen-dependent dose–response analysis, two-way ANOVA was performed using oxygen condition and compound concentration as factors. A confirmed R3ACT response required a statistically significant increase versus the corresponding control in the same biosensor readout and response direction across two independent screening runs using one-way ANOVA followed by Dunnett's post hoc test. Throughout, N denotes the number of independent replicates and n denotes the number of individual cells analyzed per replicate; corresponding values are given in each figure legend. Statistical significance is denoted as follows: ns, $p > 0.05$; *, $p \leq 0.05$; **, $p \leq 0.01$; ***, $p \leq 0.001$; and ****, $p \leq 0.0001$.

2.9. Deep Learning–Based Image Processing and Single-Cell Quantification

All image analysis scripts were developed in Python (v3.9) using the PyCharm IDE and executed on a GPU-enabled workstation (NVIDIA RTX 3070 Laptop GPU) to accelerate segmentation. Live-cell fluorescence images were acquired on a Zeiss microscope and saved as .czi files, including single-channel readouts and dual-excitation ratiometric sensors (cytosolic and mitochondria-targeted HyPer7.2) in transgenic keratinocytes. Cells were segmented using Cellpose (Stringer et al., 2021), a deep learning–based cyto-family model, applied to a normalized copy of the fluorescence image (0–1 scaling with contrast rescaling), while raw fluorescence images remained unprocessed for quantification. The Cellpose flow_threshold parameter was selected by trial-and-error using representative training images from our keratinocyte datasets to balance sensitivity and mask quality. For each Cellpose label (cell) and each channel, the mean raw intensity inside the mask was measured; background was estimated as the median raw intensity in non-cell regions, and background-subtracted intensity was defined as (cell mean − background). To reduce inclusion of unhealthy cells and segmentation artifacts, objects were filtered using morphology-based quality control, excluding small objects (minimum area threshold) and highly circular objects (circularity threshold, computed as $4\pi A/P^2$). For dual-channel datasets, per-cell ratios were computed from background-subtracted values as HyPer-high/HyPer-low. For traceability and manual QC if needed, each retained cell was assigned a sequential ID (Cell_ID_kept), and the same ID was printed on the segmentation overlay image to directly match cells to their corresponding rows in the per-cell spreadsheet. The pipeline exported two Excel tables per experiment: a per-cell table (snap name, condition path, cell ID, background-subtracted intensities, ratio) and a per-image table summarizing cell count and mean background-subtracted intensities and ratios for each snap. The NumPy, pandas, scikit-image, tifffile, matplotlib, aicspylibczi, Cellpose, and openpyxl Python libraries used were used for image analysis.

3. Results

3.1. Intended context of use and R3ACT workflow for animal-free chemical safety assessment

R3ACT was developed as an early-stage animal-free NAM workflow for mechanistic profiling of chemical-induced redox perturbation and antioxidant-response activation under physiological oxygen. The intended context of use is compound prioritization and mechanistic support within chemical safety assessment, rather than standalone regulatory hazard classification. The workflow uses three human HaCaT reporter cell lines expressing cytosolic HyPer7.2, mitochondrial HyPer7.2, or POINTER/Nrf2. Cells are adapted to 5 kPa O_2 before screening to reduce oxygen-driven artifacts. Candidate compounds are first evaluated by viability testing to define a low-cytotoxicity concentration window. Within this window, plate reader measurements identify reproducible changes in HyPer7.2 or POINTER/Nrf2 readouts. Selected responses are then assessed by oxygen-controlled high-content microscopy and Cellpose-assisted single-cell analysis. This two-stage structure is intended to generate interpretable mechanistic information that can support NAM-based prioritization and future NGRA-oriented workflows (Fig. 1).

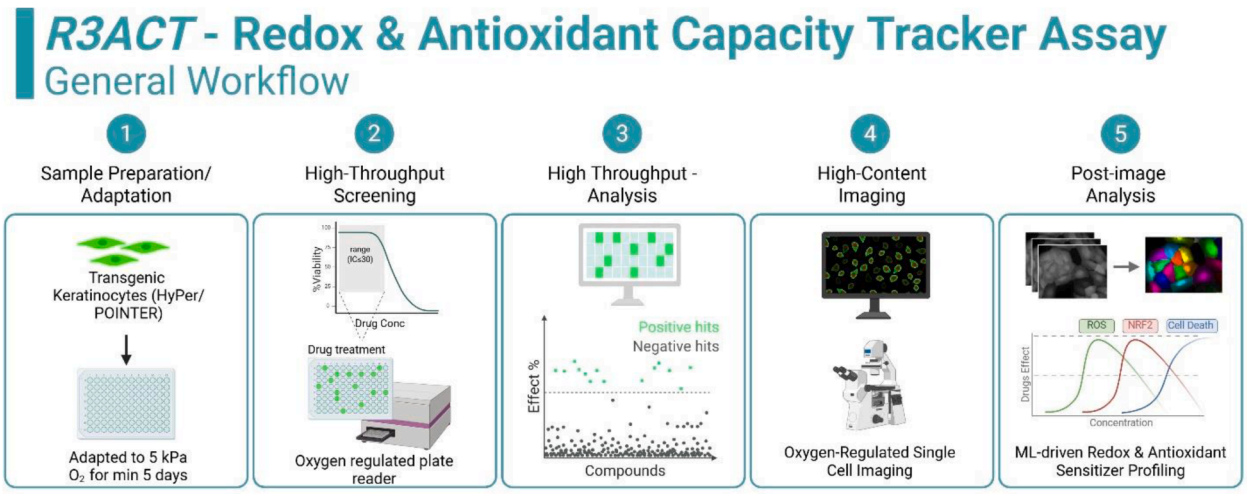

Fig. 1. Schematic of the R3ACT workflow for redox and antioxidant capacity tracker assay. (1) Sample preparation and adaptation: Immortalized human keratinocytes (HaCaT cells) stably expressing the HyPer7.2 redox biosensor (mitochondria- and cytosol-targeted) and the POINTER reporter (for Nrf2 pathway activity), respectively, are cultured at physiological oxygen (5 kPa) for at least five days prior to screening. (**2**) High-throughput screening: The oxygen-adapted cells are treated with test compounds within a predefined low-cytotoxicity concentration range, established by prior viability testing, and biosensor fluorescence signals are recorded in an oxygen-controlled plate reader environment. (**3**) Response classification: A dedicated analysis pipeline identifies treatment conditions that produce reproducible increases in HyPer7.2 and/or POINTER/Nrf2 readouts within the low-cytotoxicity test window. (**4**) High-content imaging: Selected treatment conditions are imaged at single-cell resolution under physiological oxygen conditions (5 kPa) to capture detailed HyPer7.2 and POINTER signals within mitochondria and cytosol. (**5**) Post-image data analysis: Deep-learning-based analysis of the single-cell imaging data is used to profile distinct redox and antioxidant response patterns across the cell population.

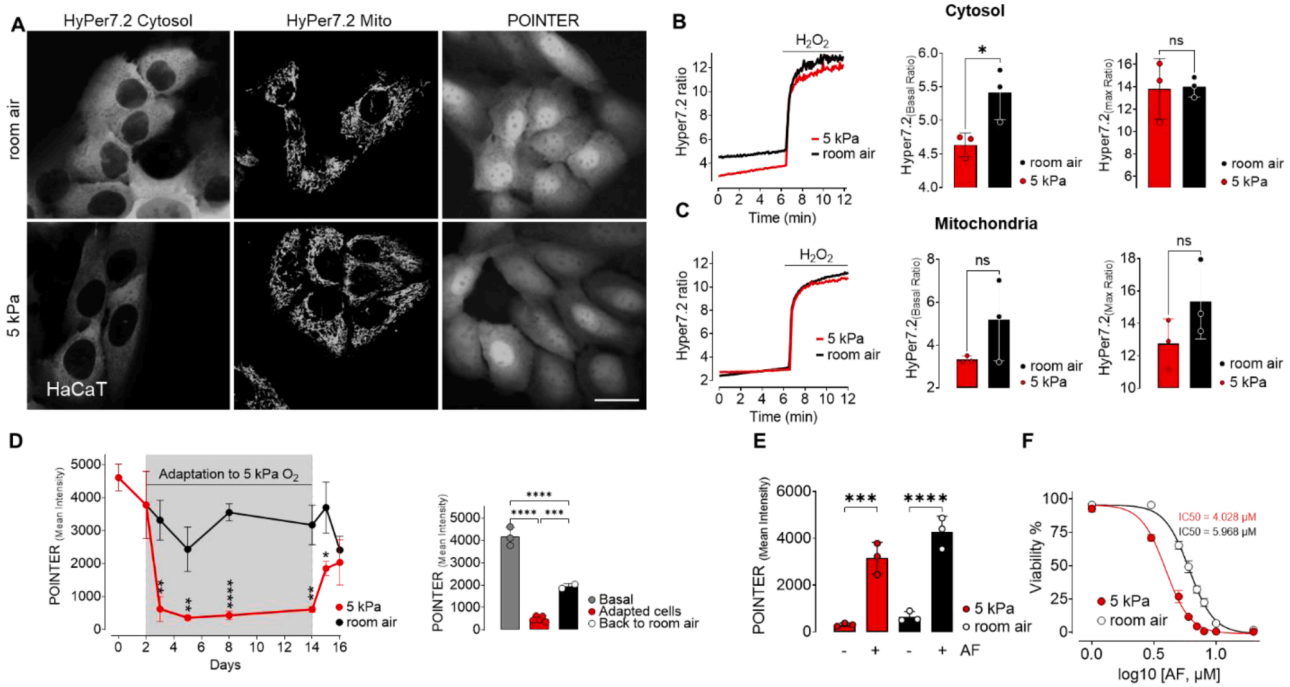

Fig. 2. Functionality test of stable HaCaT lines under physiological oxygen conditions. Red = cells adapted 5 days to 5 kPa O_2; black = cells kept in room air (~20 kPa O_2). (**A**) High-resolution representative images of HaCaT cells stably expressing Cytosolic HyPer7.2-cytosol (left), mitochondrial HyPer7.2 (middle), or POINTER (right) after adaptation to the indicated pericellular O_2 levels. Scale bar = 20 µm (**B**) Live-cell imaging of HyPer7.2-cytosol after 100 µM H_2O_2 administration. Bars: basal ratio (middle) and maximal response (right). Statistics: unpaired two-tailed Student's t-test. Data are mean ± SD. (**C**) Live-cell imaging of mitochondrial HyPer7.2 after 100 µM H_2O_2 administration, with basal and maximal responses quantified as in (B). Same statistics and data presentation as (B). N = 3. (**D**) POINTER adaptation to 5 kPa O_2. Left: time course of mean fluorescence (± SD) during days 0–16 versus room-air controls. Right: mean intensity at baseline, after 5 kPa O_2 adaptation, and after re-adaptation to room air O_2. Left panel comparison between 5 kPa and room air via the unpaired two-tailed Student's t-test, N/n = 3/20. Right panel used the one-way ANOVA with Tukey's post hoc. (**E**) POINTER response to 1 µM auranofin (AF) in room-air versus 5 kPa O_2–adapted cells. Asterisks mark between-group differences, one-way ANOVA Tukey's post-test (***P < 0.001).N/n = 3/20. (F) Viability of room-air and 5 kPa O_2–adapted HaCaT cells across AF doses, assessed by TO-PRO-3 staining and flow cytometry (IC_{50} shown on the plot).). N = 3/20,000 All error bars represent mean ±SD.

3.2. Characterizing the R3ACT biosensor cell lines under physiological oxygen conditions

We first generated transgenic HaCaT cell lines using lentiviral vectors for HyPer7.2 targeted to the cytosol or mitochondria (Fig. S2), and the POINTER reporter for Nrf2 pathway activity. High resolution wide field imaging confirmed robust expression and appropriate subcellular localization of each reporter in cells maintained in room air (~20 kPa O_2) or after adaptation to physiological oxygen (5 kPa O_2) (Fig. 2A). We next tested whether oxygen adaptation alters biosensor performance. Upon acute administration of 100 μM H_2O_2, cytosolic HyPer7.2 showed a rapid ratiometric increase under both oxygen conditions, indicating that reporter responsiveness was maintained after 5 kPa adaptation (Fig. 2B). Basal cytosolic HyPer7.2 ratios showed a modest oxygen-dependent difference in the analyzed dataset, whereas maximal responses to exogenous H_2O_2 were comparable. Mitochondrial HyPer7.2 did not show a significant oxygen-dependent difference in basal ratio or maximal response under the same challenge conditions (Fig. 2C). Moreover, because Nrf2 signaling is sensitive to ambient oxygen, as shown in previous work (Miri et al., 2025), we quantified POINTER behavior during oxygen adaptation. POINTER baseline fluorescence decreased during adaptation to 5 kPa O_2 compared with room-air controls, consistent with oxygen-dependent regulation of basal Nrf2 reporter activity (Fig. 2D). Because absolute fluorescence intensity can vary between experimental days POINTER responses were interpreted using within-experiment controls. Finally, we evaluated assay responsiveness using auranofin (AF) as a model redox-active compound. AF at 1 μM induced a clear POINTER/Nrf2 reporter response in both room-air and 5 kPa–adapted cells (Fig. 2E), confirming that antioxidant-response activation remained detectable under physiological oxygen. In parallel, AF dose–response viability testing revealed an oxygen-dependent cytotoxicity shift, with greater sensitivity at 5 kPa O_2 (IC_{50} = 4.028 μM) compared with room air (IC_{50} = 5.968 μM) (Fig. 2F). This increased sensitivity at 5 kPa O_2 was also observed for additional compounds including a non-sensitizer (salicylic acid, SA), a strong sensitizer (4-methylaminophenol sulfate, Metol), and an extreme sensitizer (1-chloro-2,4-dinitrobenzene, CDNB) (Supplementary Fig. S3). Together, these data establish functional reporter lines for R3ACT and support oxygen tension as an important experimental variable that can influence not only the reporter baseline and response interpretation but also the drug/compound sensitivity.

3.3. Pilot characterization of response kinetics and conservative response classification

AF was used as a model redox-active compound to characterize

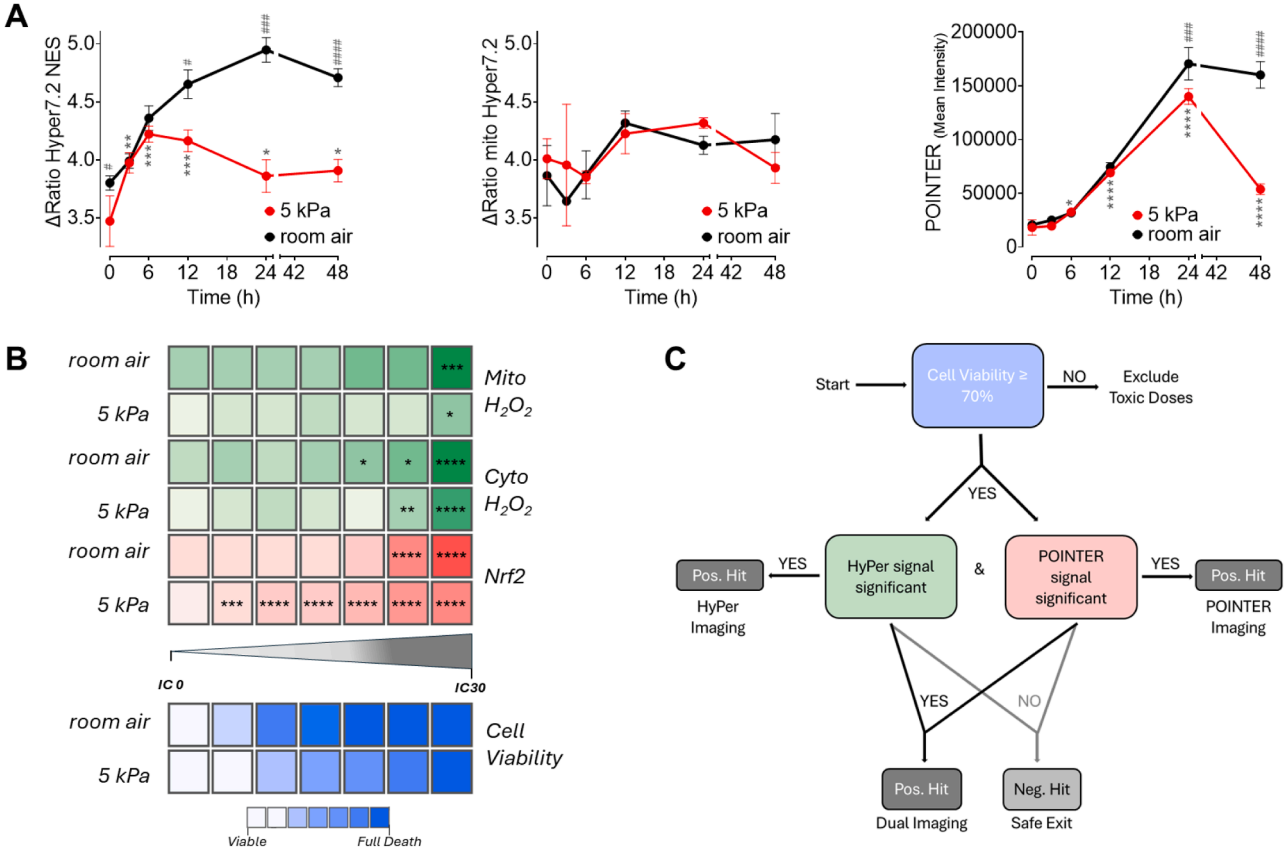

Fig. 3. R3ACT screening readouts and decision workflow illustrated. (A) Time-course responses of the biosensors following treatment with auranofin (AF; 1 μM) in stable HaCaT reporter lines. Curves show HyPer7.2 responses in the cytosol and mitochondria and the POINTER Nrf2 reporter signal over hours. Measurements were performed under room air and physiological oxygen (5 kPa O_2) conditions; red curves indicate data from 5 kPa O_2–adapted cells (room-air curves shown for comparison. # indicates a significant difference between 5 kPa O_2 and room air at the same concentration and * indicates a significant difference within the 5 kPa O_2 condition (red curve) compared with the baseline (time 0) (one-way ANOVA with Tukey's multiple-comparisons test).. Error bars represent ±SD. (**B**) Output of the custom-built R3ACT statistical analysis pipeline. Heatmap-style summary of concentration-dependent effects within the predefined low-cytotoxicity concentration range defined from viability measurements. Green boxes indicate HyPer7.2/H_2O_2 readouts, red boxes indicate POINTER/Nrf2 readouts, and blue boxes indicate viability loss determined by flow cytometry in separate range-finding experiments. For each readout, upper rows show results obtained in room air, and lower rows show responses after adaptation to 5 kPa O_2. Asterisks denote statistical significance relative to control using one-way ANOVA with Dunnett's multiple-comparison test. Confirmed responses required reproducibility across independent runs as described in the Methods. (**C**) Decision algorithm for executing R3ACT as described in the text. All error bars represent mean ±SD. N = 3.

reporter kinetics and define measurement windows for the proof-of-concept workflow (Fig. 3A, Supplementary Fig. S4). In the present setup, AF induced a stronger and more reproducible POINTER/Nrf2 response than HyPer7.2 responses. Cytosolic HyPer7.2 changes were detectable but smaller in magnitude, whereas mitochondrial HyPer7.2 responses were limited. These observations informed the use of 6 h as the HyPer7.2 measurement window and 24 h as the POINTER/Nrf2 measurement window for subsequent proof-of-concept screening.

We next applied a conservative response-classification workflow to convert multiparametric dose-dependent data into interpretable screening summaries (Fig. 3B,C). Viability testing was performed separately before reporter screening and was used to define the low-cytotoxicity concentration window. Within this window, HyPer7.2 and POINTER/Nrf2 responses were measured by plate reader and summarized as heatmap-style response maps. A confirmed R3ACT response required a statistically significant increase versus control that was reproduced in the same readout and same direction across two independent screening runs. Responses detected in only one run, or not reproduced in the same or adjacent concentration range, were classified as borderline. Selected confirmed or borderline responses were then assessed by oxygen-controlled high-content microscopy and Cellpose-assisted single-cell analysis. This workflow is intended for proof-of-concept mechanistic prioritization and should not be interpreted as a validated prediction model.

3.4. Proof-of-concept screening of exposure-relevant materials under physiological oxygen

Based on the oxygen-dependent reporter behavior observed in the pilot experiments, proof-of-concept R3ACT screening was performed in cells adapted to 5 kPa O_2. The selected materials were used as exposure-relevant examples rather than as a formal sensitization reference panel. They included PFOA as a representative PFAS, polystyrene nanoparticles (PS-NP) as a particulate exposure model, ZnO as a metal oxide material relevant to consumer-product exposure, salicylic acid as a non-sensitizer with known relevance in skin-assay discussions, and two intravenous iron formulations as pharmaceutical case examples. Viability-guided concentration selection was performed before biosensor screening, and the corresponding viability curves are shown in Supplementary Fig. S5. HyPer7.2 responses in the cytosol and mitochondria were quantified at the standardized 6 h endpoint, and POINTER/Nrf2 responses were quantified at 24 h. All plate reader experiments were performed in at least two independent rounds with technical triplicates per compound per round. Reproducible responses were dominated by POINTER/Nrf2 activation, whereas HyPer7.2 responses were smaller and did not consistently meet the confirmed-response criterion across the tested materials. PFOA showed non-reproducible responses and was therefore classified as borderline. Salicylic acid induced POINTER/Nrf2 reporter activation under physiological oxygen; because salicylic acid is not considered a skin sensitizer, this response was interpreted as antioxidant-response engagement rather

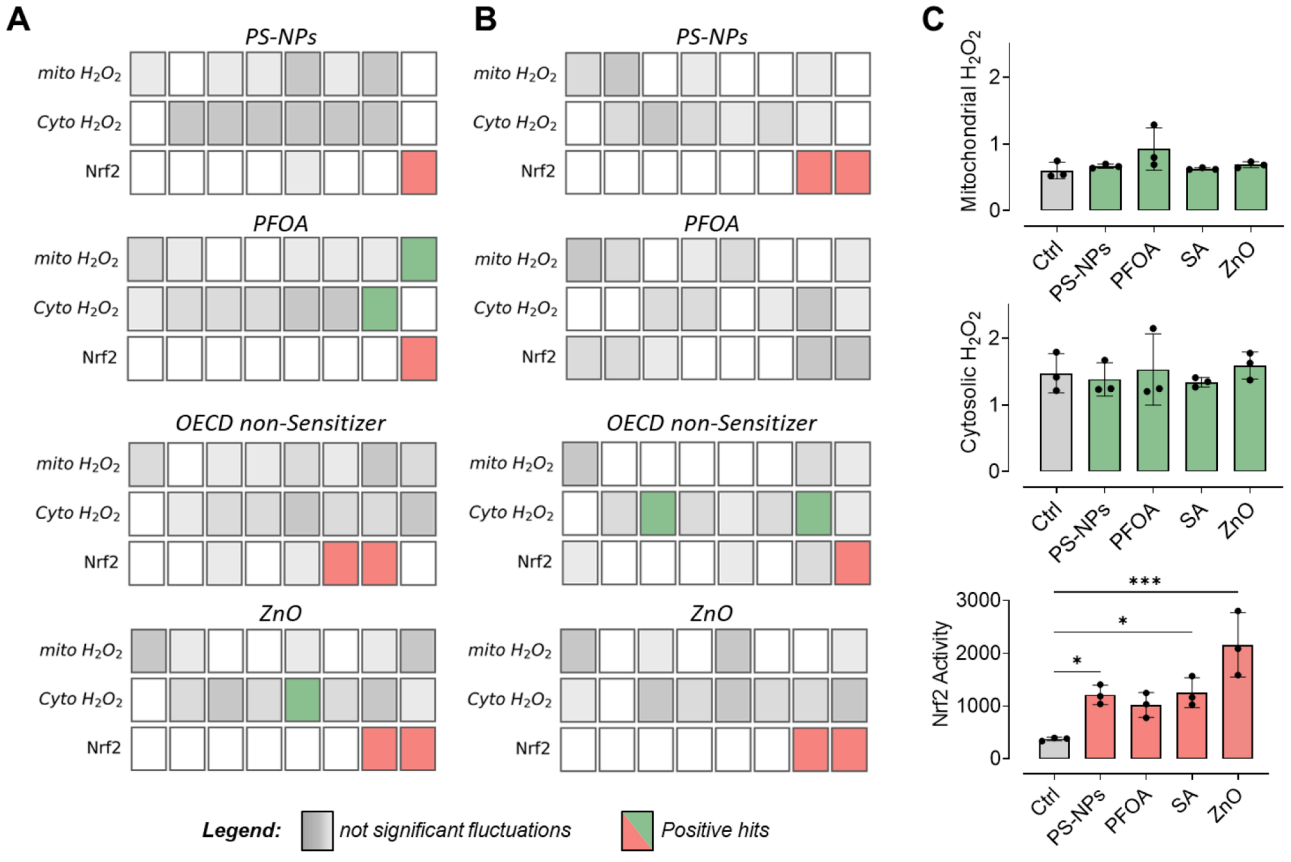

Fig. 4. Proof-of-concept R3ACT screening and microscopy confirmation of selected responses. (A, B) Heatmap-style plate reader summaries show HyPer7.2 and POINTER/Nrf2 responses in cells adapted to 5 kPa O_2 within the predefined low-cytotoxicity test range. Grayscale indicates non-significant response magnitude, while colored squares indicate statistically significant increases versus vehicle control in the corresponding run. Green indicates HyPer7.2/H_2O_2 readouts and red indicates POINTER/Nrf2 readouts. Responses were classified as confirmed only when reproduced in the same readout and same direction across independent runs; non-reproducible responses were classified as borderline. All plate reader experiments were performed in at least two independent rounds. **(C)** High-content microscopy confirmation was performed for selected conditions versus control. Bars show mean ± SD, with dots indicating 3 independent replicates. Statistical analysis was performed using one-way ANOVA with Dunnett's post hoc test. Actual tested concentrations are indicated in the panels or in Table 1. All error bars represent mean ±SD. N=3.

than as a sensitization-positive classification. Selected confirmed or borderline responses were assessed by high-content microscopy versus control (Fig. 4C). Borderline plate reader responses were not supported at single-cell level, including the PFOA/POINTER response.

To further assess whether oxygen tension influenced concentration-dependent biosensor behavior, dose–response profiles were compared between room air and 5 kPa O_2-adapted cells using two-way ANOVA with oxygen condition and compound concentration as factors (Supplementary Fig. S5). This analysis showed that oxygen tension modulated the concentration–response relationship for several readouts, with oxygen × concentration interactions observed most prominently in the Nrf2 reporter arm. In contrast, HyPer7.2 responses were generally smaller and showed fewer oxygen-dependent changes across the tested concentration ranges.

A similar proof-of-concept workflow was applied to iron formulations (Supplementary Fig. S6). Iron sucrose (IS) and ferric carboxymaltose (FCM) were screened within the predefined low-cytotoxicity concentration range and assessed by microscopy at selected concentrations based on the viability-gated workflow. Single-cell analysis was performed using the Cellpose-based workflow described in the Methods (Supplementary Fig. S8).

4. Discussion

In this study, we present R3ACT as an early-stage, animal-free NAM workflow for mechanistic profiling of chemical-induced redox perturbation and antioxidant-response activation under physiological oxygen. The workflow combines viability-gated concentration selection, genetically encoded live-cell biosensors, oxygen-controlled plate reader screening, high-content microscopy, and Cellpose-assisted single-cell analysis (Stringer et al., 2021). In the context of the roadmap toward animal-free chemical safety assessment, the main contribution of R3ACT is not regulatory hazard classification, but the generation of interpretable mechanistic information that can support compound prioritization, follow-up testing, and NGRA-oriented weight-of-evidence approaches (Berggren et al., 2017; Nelson et al., 2024).

Existing regulatory non-animal sensitization assays such as KeratinoSens™ (OECD, 2024) are built around a single pathway readout (ARE–Nrf2) using a luciferase reporter, in which signal detection requires addition of a luciferase substrate and is typically measured as a luminescence endpoint rather than a continuous, live-cell, multiparameter readout (Emter et al., 2010). While this is powerful for a standardized hazard call, it leaves a clear technology gap for mechanistic, time-resolved profiling of redox biology—distinguishing early ROS generation from later corresponding antioxidant transcriptional activation and resolving whether ROS arises in the cytosol or mitochondria. A second limitation is that these assays, like most cell-based screening, are usually performed under atmospheric room-air oxygen, even though physiological tissue O_2 is far lower and strongly shapes redox tone and stress signaling (Keeley and Mann, 2019). This is particularly relevant for skin models, where oxygen levels in the epidermal microenvironment are low and standard "normoxic" incubator conditions can drive non-physiological oxidative stress and altered cell function (Chettouh-Hammas et al., 2023). R3ACT is designed to close both gaps: it profiles compartment-resolved H_2O_2 dynamics and Nrf2 activation in parallel, in live cells, under physiological oxygen. This distinction is important because roadmap-oriented animal-free safety assessment will likely require multiple forms of evidence, including mechanistic, exposure-relevant, and context-specific information, rather than reliance on a single assay endpoint (Westmoreland et al., 2022; Nelson et al., 2024; OECD, 2025).

The present data support oxygen tension as an important experimental variable in redox- and Nrf2-based NAM workflows. Cells maintained under room air and cells adapted to 5 kPa O_2 differed in POINTER basal reporter behavior and response kinetics, indicating that ambient oxygen can influence assay interpretation. Consistent with this, cells adapted to 5 kPa O_2 showed lower basal HyPer7.2 signals. However, this baseline shift more likely reflects an adapted antioxidant network set-point under physiological oxygen, of which lower basal H_2O_2 is only one component. (Keeley and Mann, 2019; Chettouh-Hammas et al., 2023; Chettouh-Hammas and Grillon, 2024).

Importantly, the value of physiological oxygen extends beyond Nrf2 itself to the broader antioxidant regulatory network. Ambient air also biases the redox state of Nrf2 regulators such as the repressor *Bach1*, whose redox-sensitive DNA binding is better preserved under physiological oxygen (Chapple et al., 2016; Tossounian et al., 2025). Low-oxygen conditions therefore may better reflect the native regulation of antioxidant-response (Chettouh-Hammas et al., 2023). These findings support the need to control and report oxygen conditions when developing animal-free *in vitro* methods for chemical safety assessment.

AF was useful as a pilot compound to characterize response kinetics and define measurement windows, particularly for POINTER/Nrf2 activation (Dunigan et al., 2018). Also, AF inhibits thioredoxin reductase, thereby impairing thioredoxin-dependent peroxide detoxification and promoting intracellular H_2O_2 accumulation. Consistent with this mechanism, we previously showed that acute AF administration increases the HyPer7.2 ratio in hCMEC/D3 cells (Miri et al., 2025), and in EA.hy926 cells (Altun et al., 2024). This is consistent with our data where we further show that AF incubation increases the HyPer7.2 response in HaCaT cells. After confirming AF's effect on both readouts, characterizing its response kinetics defined the measurement windows for R3ACT. These kinetics indicated that Nrf2 activation and H_2O_2 elevation occur before 48 h, so a fixed late endpoint could miss transient or earlier redox-associated events. R3ACT therefore uses a 6 h HyPer7.2 readout to capture earlier compartment-resolved H_2O_2 changes and a 24 h Nrf2 readout to assess downstream antioxidant-response activation.

In the present experimental setup, the tested compounds elicited prominent POINTER responses, whereas HyPer7.2 signals remained negligible. This does not indicate lower sensitivity of HyPer7.2, but rather the absence of transient H_2O_2 generation in response to these compounds. The two reporters differ fundamentally in mechanism and timescale: HyPer7.2 is a direct, reversible, real-time sensor of instantaneous intracellular H_2O_2, whereas POINTER is a transcriptional reporter that integrates and amplifies a downstream antioxidant-response signal over many hours. A modest but sustained H_2O_2 change can therefore produce a non-significant HyPer7.2 readout while still driving a strong, amplified POINTER response.

To avoid overinterpretation of isolated statistical events, we applied a conservative reproducibility rule. Responses observed in both independent runs in the same readout and direction were classified as confirmed, whereas responses observed in only one run or at inconsistent concentrations were classified as borderline. This approach is appropriate for a proof-of-concept workflow but should not be considered a validated prediction model. This limitation partly reflects the absence of established reference thresholds for oxygen-controlled, multiparametric redox/Nrf2 profiling under physiological oxygen. Existing reference classifications and performance standards were developed for established assay formats such as ARE-Nrf2 luciferase methods (OECD, 2015, 2024), not for live-cell biosensor workflows combining physiological oxygen control, compartment-resolved H_2O_2 readouts, and Nrf2 reporter activation. Therefore, future studies should establish R3ACT-specific acceptance criteria, quantitative response thresholds, and reference-compound benchmarking before broader screening or regulatory applicability can be assessed (Nelson et al., 2024).

The selected materials should be interpreted as proof-of-concept and exposure-relevant examples rather than as a formal sensitization validation panel. PFOA, PS-NP, ZnO, salicylic acid, and iron formulations represent different chemical or material classes relevant to consumer-product, environmental, or pharmaceutical exposure. Within this limited set, reproducible responses were mainly observed in the POINTER/Nrf2 arm. The salicylic acid response should be interpreted as

antioxidant-response engagement under physiological oxygen, not as evidence of sensitization potential. This distinction is central to the intended context of use of R3ACT as a mechanistic profiling workflow rather than a binary regulatory classifier (Chettouh-Hammas and Grillon, 2024; OECD, 2024; Miri et al., 2025).

In R3ACT, iron sucrose (IS) showed reproducible POINTER/Nrf2 activation across two independent screening runs, and this response was supported by high-content single-cell imaging at the selected low-cytotoxicity concentration. In contrast, ferric carboxymaltose (FCM) did not show a comparable Nrf2 response in the present workflow. Neither formulation produced a reproducible increase in HyPer7.2 ratio within the tested concentration window. However, IS increased cytosolic H_2O_2 levels compared with the control, suggesting a formulation-dependent redox trend that did not meet the confirmed response criterion. These findings illustrate how R3ACT can distinguish formulation-dependent antioxidant-response engagement under physiological oxygen, while also showing that Nrf2 activation can occur without a confirmed HyPer7.2 response at the selected endpoint. The present dataset also illustrates that Nrf2 activation and detectable H_2O_2 increases do not necessarily coincide at the selected measurement endpoints (Miri et al., 2025). Many conditions produced POINTER/Nrf2 responses without reproducible HyPer7.2 increases. This is expected, because the H_2O_2–Nrf2 relationship is not one-to-one: Nrf2 integrates upstream signaling over time and can also be activated by redox-independent routes that do not raise intracellular H_2O_2. A transient or efficiently buffered H_2O_2 change may therefore leave little standing HyPer7.2 signal while still engaging Nrf2.

In its intended context of use, R3ACT functions as a mechanistic prioritization tool rather than a hazard classifier, and the biosensor readouts are therefore not used to label a compound as "safe" or "toxic." Instead, four interpretable patterns can be distinguished. A combined HyPer7.2$^+$/POINTER$^+$ response indicates both an intracellular H_2O_2 increase and downstream Nrf2 activation, the signature most consistent with redox-driven antioxidant-response engagement and identifies high-priority candidates for mechanistic follow-up on oxidative distress. A HyPer7.2$^-$/POINTER$^+$ pattern indicates Nrf2 engagement without a confirmed H_2O_2 increase; pointing toward antioxidant-response activation through routes that are not necessarily H_2O_2-mediated. Salicylic acid is a candidate example of this pattern in the present dataset; a plausible mechanism is the activation of AMPK by salicylic acid (Hawley et al., 2012), which can in turn promote Nrf2-dependent transcription through several routes (Fischhuber et al., 2020; Petsouki et al., 2023). A HyPer7.2$^+$/POINTER$^-$ pattern would indicate an intracellular H_2O_2 increase that has not, at the tested dose and timepoint, triggered a measurable adaptive antioxidant response; this is not in itself an indicator of toxicity, but flags a redox perturbation that may outpace or bypass adaptive Nrf2 signaling and warrants follow-up on dose and kinetics. Finally, a HyPer7.2$^-$/POINTER$^-$ result indicates no detectable engagement of either readout within the non-cytotoxic window, deprioritizing the compound for H_2O_2- and Nrf2-related mechanisms under the tested conditions.

Within the NAM lifecycle, R3ACT is currently positioned at the method-development and early application stage and is not presented as a validated method. Moving R3ACT toward regulatory acceptance, including potential OECD adoption, would require a formal validation process addressing the elements established for such methods: defined performance standards and acceptance criteria (for reporter dynamic range, assay robustness, and reproducibility), harmonized SOPs for oxygen control, cell adaptation, plate reader acquisition, image acquisition, and data analysis, fixed and versioned analysis scripts, benchmarking against agreed reference chemical panels such as those in the SkinSensDB database (Wang et al., 2017), and formal inter-laboratory studies to establish reproducibility and quantify between-laboratory variability. Only once these validation requirements are met should regulatory applicability or integration into defined approaches be assessed.

5. Conclusion

R3ACT provides an animal-free, oxygen-controlled live-cell workflow for mechanistic profiling of intracellular H_2O_2 dynamics and Nrf2-dependent antioxidant-response activation. The present study establishes feasibility of the workflow using human keratinocyte reporter lines, viability-gated compound testing, plate reader screening, high-content microscopy, and Cellpose-assisted single-cell analysis. In its current form, R3ACT should be regarded as an early-stage NAM that can support chemical prioritization and NGRA-oriented mechanistic evidence generation, not as a validated regulatory assay. Further reference-compound benchmarking, predefined performance criteria, serum-free adaptation, and inter-laboratory studies will be required to assess its role in future animal-free chemical safety assessment strategies.

Declaration of generative AI and AI-assisted technologies in the manuscript preparation process

During the preparation of this work, the authors used ChatGPT (OpenAI) and Claude (Anthropic) to assist with grammar correction, language refinement, clarity, and organization of the manuscript text. ChatGPT was also used to support code writing and code refinement for data processing and analysis workflows. These tools were not used to generate experimental data, perform statistical analyses independently, or draw scientific conclusions. After using these tools, the authors reviewed and edited all outputs as needed and take full responsibility for the content of the published article.

CRediT authorship contribution statement

Joudi Armouch: Writing – review & editing, Writing – original draft, Visualization, Software, Methodology, Investigation, Formal analysis, Data curation. **Hamzah Issa:** Writing – review & editing, Methodology, Investigation. **Emre Vatandaşlar:** Writing – review & editing, Investigation. **Sena Yildirim:** Writing – review & editing, Methodology. **Seyed Mohammad Miri:** Writing – review & editing, Methodology. **Asel Aydeger:** Writing – review & editing, Methodology. **Asal Ghaffari Zaki:** Writing – review & editing, Methodology. **Melike Secilmis:** Writing – review & editing, Investigation. **Kıvanç Kök:** Writing – review & editing, Formal analysis. **Ahmet Kaplan:** Software. **Theresa Balber:** Writing – review & editing, Methodology. **Thomas Birngruber:** Writing – review & editing. **Ahmet Katı:** Writing – review & editing, Resources, Conceptualization. **Emrah Eroglu:** Writing – review & editing, Visualization, Validation, Supervision, Resources, Project administration, Funding acquisition, Conceptualization.

Declaration of competing interests

The authors declare the following financial interests/personal relationships which may be considered as potential competing interests:

Emrah Eroglu reports financial support was provided by Scientific and Technological Research Council of Turkey. Emrah Eroglu reports financial support was provided by European Molecular Biology Organization. Joudi Armouch has patent pending to Istanbul Medipol University. If there are other authors, they declare that they have no known competing financial interests or personal relationships that could have appeared to influence the work reported in this paper.

Acknowledgement

Parts of this study were supported by the Installation Grant from the European Molecular Biology Organization awarded to E.E. (grant ID: EMBO IG J4113), and additional support was provided by the Career Development Program of the Scientific and Technological Research Council of Türkiye (TÜBİTAK 3501) awarded to E.E. (grant ID: 222S258).

Supplementary materials

Supplementary material associated with this article can be found, in the online version, at doi:10.1016/j.namjnl.2026.100117.

Data availability

Cell lines, plasmids, codes and the raw data supporting the findings of this study are available from the corresponding author upon reasonable request.

References

Altun, H.Y., Secilmis, M., Yang, F., et al., 2024. Visualizing hydrogen peroxide and nitric oxide dynamics in endothelial cells using multispectral imaging under controlled oxygen conditions. Free Radical Biology and Medicine 221, 89–97. https://doi.org/10.1016/j.freeradbiomed.2024.05.021.

Barakat, S., Yang, F., Yelkenci, H.E., et al., 2025. Proteomic Data and Drug Implications for Cerebral Microvascular Endothelial Cells Under Varying Oxygen Levels. Sci Data 12, 989. https://doi.org/10.1038/s41597-025-05160-z.

Berggren, E., White, A., Ouedraogo, G., et al., 2017. Ab initio chemical safety assessment: A workflow based on exposure considerations and non-animal methods. Comput Toxicol 4, 31–44. https://doi.org/10.1016/j.comtox.2017.10.001.

Chapple, S.J., Keeley, T.P., Mastronicola, D., et al., 2016. Bach1 differentially regulates distinct Nrf2-dependent genes in human venous and coronary artery endothelial cells adapted to physiological oxygen levels. Free Radic Biol Med 92, 152–162. https://doi.org/10.1016/j.freeradbiomed.2015.12.013.

Chettouh-Hammas, N., Grillon, C., 2024. Physiological skin oxygen levels: An important criterion for skin cell functionality and therapeutic approaches. Free Radic Biol Med 222, 259–274. https://doi.org/10.1016/j.freeradbiomed.2024.06.015.

Chettouh-Hammas, N., Fasani, F., Boileau, A., et al., 2023. Improvement of Antioxidant Defences in Keratinocytes Grown in Physioxia: Comparison of 2D and 3D Models. Oxid Med Cell Longev 2023, 6829931. https://doi.org/10.1155/2023/6829931.

Dunigan, K., Li, Q., Li, R., et al., 2018. The thioredoxin reductase inhibitor auranofin induces heme oxygenase-1 in lung epithelial cells via Nrf2-dependent mechanisms. Am J Physiol Lung Cell Mol Physiol 315, L545–L552. https://doi.org/10.1152/ajplung.00214.2018.

Emter, R., Ellis, G., Natsch, A., 2010. Performance of a novel keratinocyte-based reporter cell line to screen skin sensitizers in vitro. Toxicol Appl Pharmacol 245, 281–290. https://doi.org/10.1016/j.taap.2010.03.009.

Eroğlu, E., 2024. A Call for Innovation in Drug Screening: Integrating Genetically Encoded Biosensors for Deeper Insights. Abant Med J 13, 45–46. https://doi.org/10.47493/abantmedj.1529498.

Fentem, J., Malcomber, I., Maxwell, G., et al., 2021. Upholding the EU's Commitment to 'Animal Testing as a Last Resort' Under REACH Requires a Paradigm Shift in How We Assess Chemical Safety to Close the Gap Between Regulatory Testing and Modern Safety Science. Altern Lab Anim 49, 122–132. https://doi.org/10.1177/02611929211040824.

Fischer, K., 2015. Animal Testing and Marketing Bans of the EU Cosmetics Legislation. European Journal of Risk Regulation 6, 613–621. https://doi.org/10.1017/S1867299X00005158.

Fischhuber, K., Matzinger, M., Heiss, E.H., 2020. AMPK Enhances Transcription of Selected Nrf2 Target Genes via Negative Regulation of Bach1. Front Cell Dev Biol 8, 628. https://doi.org/10.3389/fcell.2020.00628.

Franzosa, J.A., Bonzo, J.A., Jack, J., et al., 2021. High-throughput toxicogenomic screening of chemicals in the environment using metabolically competent hepatic cell cultures. npj Syst Biol Appl 7, 7. https://doi.org/10.1038/s41540-020-00166-2.

Han, J.J., 2023. FDA Modernization Act 2.0 allows for alternatives to animal testing. Artif Organs 47, 449–450. https://doi.org/10.1111/aor.14503.

Hawley, S.A., Fullerton, M.D., Ross, F.A., et al., 2012. The ancient drug salicylate directly activates AMP-activated protein kinase. Science 336, 918–922. https://doi.org/10.1126/science.1215327.

Hubrecht, R.C., Carter, E., 2019. The 3Rs and Humane Experimental Technique: Implementing Change. Animals (Basel) 9 754. https://doi.org/10.3390/ani9100754.

Keeley, T.P., Mann, G.E., 2019. Defining Physiological Normoxia for Improved Translation of Cell Physiology to Animal Models and Humans. Physiol Rev 99, 161–234. https://doi.org/10.1152/physrev.00041.2017.

Kimber, I., Weisenberger, C., 1989. A murine local lymph node assay for the identification of contact allergens. Assay development and results of an initial validation study. Arch Toxicol 63, 274–282. https://doi.org/10.1007/BF00278640.

Lu, R., 2024. Advances in Ophthalmic Organ-on-a-Chip Models: Bridging Translational Gaps in Disease Modeling and Drug Screening. International Journal of Translational Medicine 4, 710–725. https://doi.org/10.3390/ijtm4040049.

Miri, S.M., Ata, B.N., Çimen, Ş., et al., 2025. Development of an Oxygen-Insensitive Nrf2 Reporter Reveals Redox Regulation under Physiological Normoxia. ACS Sens. https://doi.org/10.1021/acssensors.4c03167.

Murphy, M.P., Bayir, H., Belousov, V., et al., 2022. Guidelines for measuring reactive oxygen species and oxidative damage in cells and in vivo. Nat Metab 4, 651–662. https://doi.org/10.1038/s42255-022-00591-z.

Nelson, C.P., Brown, P., Fitzpatrick, S., et al., 2024. Advancing alternative methods to reduce animal testing. Science 386, 724–726. https://doi.org/10.1126/science.adg6228.

Nwachukwu, I.D., Sarteshnizi, R.A., Udenigwe, C.C., et al., 2021. A Concise Review of Current In Vitro Chemical and Cell-Based Antioxidant Assay Methods. Molecules 26, 4865. https://doi.org/10.3390/molecules26164865.

OECD, 2015. Performance Standards for Assessment of Proposed Similar or Modified In Vitro Skin Sensitisation ARE-NRF2 Luciferase Test Methods. OECD Series on Testing and Assessment. https://doi.org/10.1787/9dec33ba-en.

OECD, 2024. Test No. 442D: In Vitro Skin Sensitisation: Assays addressing the Adverse Outcome Pathway Key Event on Keratinocyte activation. OECD Guidelines for the Testing of Chemicals, Section 4. https://doi.org/10.1787/9789264229822-en.

OECD, 2025. Guideline No. 497: Defined Approaches on Skin Sensitisation. OECD Guidelines for the Testing of Chemicals, Section 4. https://doi.org/10.1787/b92879a4-en.

OECD, 2025. Guideline No. 497: Defined Approaches on Skin Sensitisation. OECD Guidelines for the Testing of Chemicals, Section 4. OECD Publishing, Paris.

Pak, V.V., Ezeriņa, D., Lyublinskaya, O.G., et al., 2020. Ultrasensitive Genetically Encoded Indicator for Hydrogen Peroxide Identifies Roles for the Oxidant in Cell Migration and Mitochondrial Function. Cell Metab 31, 642–653. https://doi.org/10.1016/j.cmet.2020.02.003 e6.

Pang, Y., Zhang, H., Ai, H.-W., 2021. Genetically Encoded Fluorescent Redox Indicators for Unveiling Redox Signaling and Oxidative Toxicity. Chem Res Toxicol 34, 1826–1845. https://doi.org/10.1021/acs.chemrestox.1c00149.

Petsouki, E., Ender, S., Sosa Cabrera, S.N., et al., 2023. AMPK-Mediated Phosphorylation of Nrf2 at S374/S408/S433 Favors Its βTrCP2-Mediated Degradation in KEAP1-Deficient Cells. Antioxidants (Basel) 12, 1586. https://doi.org/10.3390/antiox12081586.

Potekhina, E.S., Bass, D.Y., Kelmanson, I.V., et al., 2020. Drug Screening with Genetically Encoded Fluorescent Sensors: Today and Tomorrow. Int J Mol Sci 22, 148. https://doi.org/10.3390/ijms22010148.

Ramirez, T., Mehling, A., Kolle, S.N., et al., 2014. LuSens: a keratinocyte based ARE reporter gene assay for use in integrated testing strategies for skin sensitization hazard identification. Toxicol In Vitro 28, 1482–1497. https://doi.org/10.1016/j.tiv.2014.08.002.

Ramirez, T., Stein, N., Aumann, A., et al., 2016. Intra- and inter-laboratory reproducibility and accuracy of the LuSens assay: A reporter gene-cell line to detect keratinocyte activation by skin sensitizers. Toxicol In Vitro 32, 278–286. https://doi.org/10.1016/j.tiv.2016.01.004.

Schmeisser, S., Miccoli, A., von Bergen, M., et al., 2023. New approach methodologies in human regulatory toxicology - Not if, but how and when! Environ Int 178, 108082. https://doi.org/10.1016/j.envint.2023.108082.

Secilmis, M., Altun, H.Y., Pilic, J., et al., 2021. A Co-Culture-Based Multiparametric Imaging Technique to Dissect Local H2O2 Signals with Targeted HyPer7. Biosensors (Basel) 11, 338. https://doi.org/10.3390/bios11090338.

Sevimli, G., Smith, M.J., Caglar, T.A., et al., 2022. Nitric oxide biosensor uncovers diminished ferrous iron-dependency of cultured cells adapted to physiological oxygen levels. Redox Biol 53, 102319. https://doi.org/10.1016/j.redox.2022.102319.

Stringer, C., Wang, T., Michaelos, M., et al., 2021. Cellpose: a generalist algorithm for cellular segmentation. Nat Methods 18, 100–106. https://doi.org/10.1038/s41592-020-01018-x.

Stuart, J.A., Fonseca, J., Moradi, F., et al., 2018. How Supraphysiological Oxygen Levels in Standard Cell Culture Affect Oxygen-Consuming Reactions. Oxid Med Cell Longev 2018, 8238459. https://doi.org/10.1155/2018/8238459.

Tiede, L.M., Cook, E.A., Morsey, B., et al., 2011. Oxygen matters: tissue culture oxygen levels affect mitochondrial function and structure as well as responses to HIV viroproteins. Cell Death Dis 2, e246. https://doi.org/10.1038/cddis.2011.128.

Tossounian, M.-A., Zhyvoloup, A., Chatterjee, R., et al., 2025. Dissecting the Interplay Between NRF2 and BACH1 at CsMBEs. Antioxidants (Basel) 14 1203. https://doi.org/10.3390/antiox14101203.

Wang, C.-C., Lin, Y.-C., Wang, S.-S., et al., 2017. SkinSensDB: a curated database for skin sensitization assays. J Cheminform 9, 5. https://doi.org/10.1186/s13321-017-0194-2.

Westmoreland, C., Bender, H.J., Doe, J.E., et al., 2022. Use of New Approach Methodologies (NAMs) in regulatory decisions for chemical safety: Report from an EPAA Deep Dive Workshop. Regulatory Toxicology and Pharmacology 135, 105261. https://doi.org/10.1016/j.yrtph.2022.105261.